Materials & Design 227 (2023) 111788

Contents lists available at ScienceDirect

Materials & Design

journal homepage: www.elsevier.com/locate/matdes

Preparation of cellulose acetate film with dual hydrophobic-hydrophilic properties using solution blow spinning

Ana Kramar *, Javier González-Benito

Department of Materials Science and Engineering and Chemical Engineering and Instituto Tecnológico de Química y Materiales "Álvaro Alonso Barba", Universidad Carlos III de Madrid, Avda. Universidad 30, 28911 Leganés, Spain

HIGHLIGHTS

- Cellulose acetate membranes are prepared using solution blow spinning from solvent mixtures containing acetone and higher boiling point solvents.
- The acetone ratio increase in a solvent mixture causes a transition from hydrophilic film to hydrophobic multi-structured membrane.
- Sequential processing of two different polymer solutions allows the preparation of a double-layered film with distinctively different sides.
- The sides of the film exhibit more than three times different roughness value and contact angle difference of 30°.
- Hydrophobic material can be prepared from a hydrophilic polymer by inducing complex morphology with high roughness using solution blow spinning.

GRAPHICAL ABSTRACT

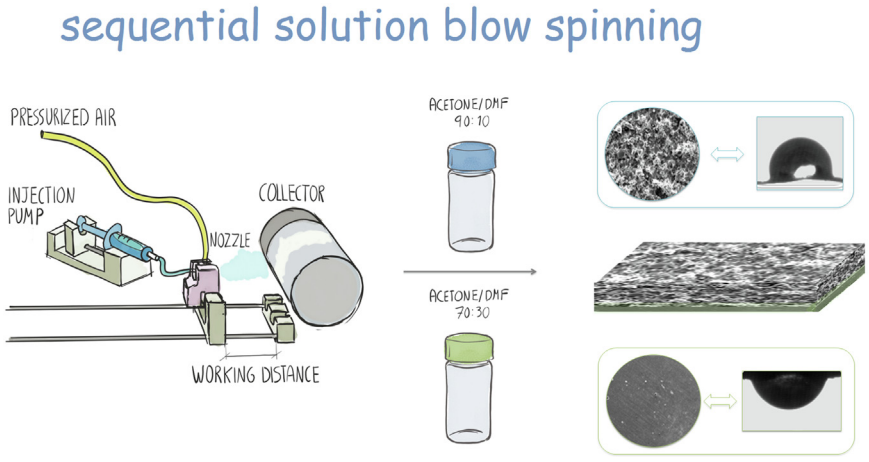

ARTICLE INFO

Article history:
Received 13 September 2022
Revised 22 February 2023
Accepted 22 February 2023
Available online 26 February 2023

Keywords:
Solution blow spinning
Cellulose acetate
Double-layered film
Dual wettability

ABSTRACT

Solution blow spinning (SBS), a processing method alternative to electrospinning, where pressured air is used instead of an electric field, was used in this work for the preparation of cellulose acetate (CA) materials. The sequential use of SBS to produce a double-layered film is also investigated. Mixtures of acetone with acetic acid or N,N-dimethylformamide (DMF) were studied as systems for polymer solution preparation. The type of produced material (flat film or multi-structured membranes constituted from submicrometric fibers with beads), its thermal properties, crystallinity, and morphology are more dependent on the solvent system than other SBS processing parameters. Roughness and porosity of differently produced materials influence wettability measured by the contact angle, which ranges in this work from approx. 69.8° ± 3° for a flat film to 104° ± 5° for fibrous material. Finally, a double-layered film, prepared by sequential SBS of individual layers different in terms of wettability, renders a standalone film of dual wettability, with one side hydrophobic and the other hydrophilic.

* Corresponding author at: Department of Material Science and Engineering and Chemical Engineering, Universidad Carlos III de Madrid, Avda. Universidad 30, 28911 Leganés, Madrid, Spain.
E-mail address: akramar@ing.uc3m.es (A. Kramar).

https://doi.org/10.1016/j.matdes.2023.111788
0264-1275/

1. Introduction

In a society with growing demand for materials prepared from natural, renewable resources, cellulose acetate (CA), a derivative of the most abundant polymer on Earth [1], becomes highly appreciated and sought. CA has excellent film and fiber-forming properties [2], making its use already familiar in sectors of fibers, films, and filters [3,4]. Great interest has grown in recent years in the case of CA nanofibrous materials, especially with the introduction of electrospinning [5–8]. CA electrospun materials already have many applications, for example in tissue engineering [9,10], filtration [11], heavy metal ion removal [12–14], wound dressings [15], and drug delivery [16–18]. Furthermore, CA research interest is also growing towards its use for food packaging [19]. In particular, electrospinning and solution casting as film-forming procedures, have been recently revived for CA, to prepare relatively thin materials with potential use as food packaging films [20–25]. CA-based materials are biodegradable, renewable, and considered safe for humans and the environment. However, for food packaging, a film should exhibit a certain degree of hydrophobicity [26]. This is one of the important concerns, especially regarding the use of hydrophilic polymers such as CA [27], because they usually present poor barrier properties against water which can lead to increased moisture in the food and consequently its quick deterioration in terms of quality and safety [26,27]. CA is less hydrophilic than cellulose due to substituted OH groups on the cellulose chain [28]; however, in the form of casted films CA has a static water contact angle of $\sim 60^{\circ}$ which includes this material in the hydrophilic range. Recently, it has been shown that it is possible to further decrease CA hydrophilicity, up to the range of hydrophobicity and even superhydrophobicity, by obtaining particular morphologies using electrospinning [29–31]. The hydrophobic behavior of electrospun CA mats was explained by the increase in surface roughness, a decrease in available hydrophilic functional groups in CA [30], and the dense packing of nanofibers [31]. On the other hand, some research presented non-hydrophobic CA materials produced using similar electrospinning conditions [7,32] as the ones which resulted in hydrophobic mats, therefore it is still not clear which conditions used during electrospinning influenced obtaining of hydrophobic or hydrophilic material. Some conclusions however can be derived. Homogenous morphology of produced CA mat can contribute to hydrophilicity [30–32], while the opposite, increased heterogeneity (existence of fibers with beads for example [32]) and increased surface roughness, leads to lower contact angles during wetting and higher hydrophobicity of produced materials. Therefore, it would be beneficial to study the possibility to obtain hydrophobic CA material by preparation of complex surface morphology. Electrospinning, ES, has a good potential to turn a hydrophilic polymer into a hydrophobic material, however, there are some drawbacks of ES (the use of a high electric field or relatively low production rates). This can be addressed by an investigation into novel techniques such as solution blow spinning (SBS) [33–38] for materials preparation. SBS is well demonstrated to be a technique for the production of nanofibers and films, comparable to electrospinning with fast processing times [8,39–41]. In SBS, a polymer solution or suspension is pumped through the inner channel of a nozzle (usually a capillary or a needle of a small diameter) while high-velocity pressurized air (typically from 0.5 to 4 bars depending on the polymer system and the device configuration) flows along the outer channel of the nozzle, exerting at its exit a force for polymer jet expulsion, and at the same time accelerating solvent removal during nanofibers formation [33]. The collector is positioned at a certain distance from the nozzle where produced material (fibers or films) is collected. SBS was introduced in 2009. [33] and up to date, it has been optimized mostly for obtaining fibrous membranes from synthetic polymers [42–45] or plain films from ethylene-vinyl acetate [46], poly(methyl methacrylate) [47], polysulfone [48], and poly(lactic-co-glycolic acid)/poly(ethylene glycol)/silver (PLGA/PEG/Ag) [49]. The possibility of SBS to promote different morphologies and consequently different properties of the film or fibrous membrane opens up this technique for the design and preparation of materials for various applications, such are filtration membranes, food packaging, biomedical materials, and wound dressings [37,38,50]. Mentioned applications, specifically in the biomedical field, are especially important since SBS enables the direct application of fibrous material to the target (e.g. body or wound).

According to recent studies, it seems there is a great challenge in processing CA using SBS. Although the first report about SBS of any polymer dates back to 2009., the use of SBS to process for the first time CA is very recent [51], where Dadol with co-authors obtained CA nanofibers using co-spinning with another polymer, polyacrylonitrile. CA, as a polymer soluble in many organic solvents, allows great variations in processing conditions, especially during preparation of films or fibers . This also implies that by changing solvents and other conditions of preparation, morphology can be tuned, and consequently wettability can also be controlled.

In this work, we provide extensive insight into the use of various solvents, concentrations, and processing parameters to prepare pure CA materials by the use of SBS. In order to understand the effect of processing conditions on the production of CA, morphology is carefully studied, as well as wettability and other important properties (thermal, structural, and physical) to finally understand the performance of these materials. In the first part of this study, we investigate a variety of different processing parameters, including solvents for polymer solution preparation and SBS parameters (injection rates and air pressure at the exit of the nozzle). Further, we choose the most optimal conditions in terms of SBS parameters, and we vary only the polymer solution composition. In this way, we can analyze how the morphology of a resulting material can be significantly altered by a simple change of the solvent system for the polymer. In this study, we also explore the possibility to process sequentially morphologically different layers of CA in order to produce a double-layered film, aiming at Janus-type of films, with distinctively different properties on each side. Janus-type of films has gained considerable interest in recent years due to their unique asymmetric properties in terms of wettability, porosity, and chemical activity [52]. According to the literature, Janus membranes are usually prepared using vapor deposition, electrospinning, spray coating, co-extrusion, and phase inversion [52–55]. The use of an SBS device for this purpose, according to the best of the author's knowledge, was not investigated.

2. Experimental

2.1. Materials

Cellulose acetate-CA (Mn 30000), acetone-Ac (HPLC > 99.9%), N, N,dimethylformamide-DMF (HPLC > 99.9%), and acetic acid-HAc (glacial), were supplied by Sigma Aldrich Merck and used as received, without further purification. To prepare solutions, CA was added to the solvent system and stirred for 24 h at room temperature. Different solvent systems were considered, pure acetone, mixtures of Ac/HAc (70:30, 50:50, 25:75) and Ac/DMF(70:30, 80:20, 90:10), with the compositions expressed in v/v %.

2.2. Solution blow spinning

A low-cost homemade device (schematic is given in Fig. 1), developed by the Group of Composite Materials and Interphases

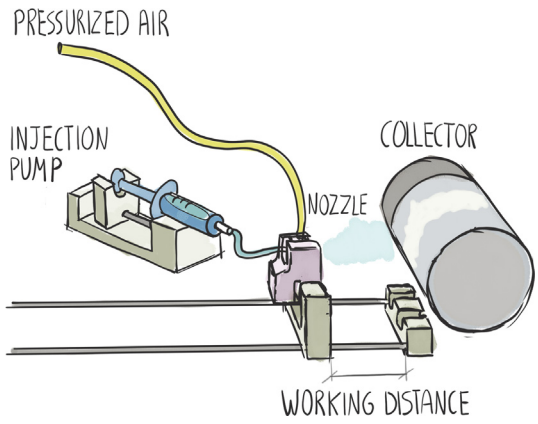

Fig. 1. Schematic representation of the solution blow spinning device with its components used in this study.

of the UC3M, was used for solution blow spinning [56]. Briefly, the device consists of a nozzle connected to the high air pressure supply, a rotating cylindrical collector with adjustable rotational speed (50–250 RPM), and an injection pump capable to provide injection rates of the CA solutions from 0.125 ml/min to 1 ml/min.

The nozzle consists of a 3D printed part that has an opening on top for air pressure supply, which delivers airflow to a channel of 2 mm diameter, through which passes the needle of 0.6 mm. The protrusion of the needle at the exit of the nozzle was set to 2 mm. A detailed schematic of the nozzle can be seen in the literature [56]. In this study, we investigate the applied air pressure in a range of 0.5–3.5 bar, depending on the polymer's solution. The environmental conditions in a laboratory set-up of the SBS device during the production of materials were monitored and performed at 22 ± 2 °C and 35 ± 5 % relative humidity.

2.3. Characterization

2.3.1. Properties of solvent system

(a) The vapor pressure of the solvent mixture (or boiling point) can directly influence the evaporation rate and therefore SBS. Estimation of a boiling point of the mixtures *T(mix)* was performed using equations (1) and (2):

$$\Delta T = i \cdot K_b \cdot m \tag{1}$$

$$T(mix) = T(solvent) + \Delta T \tag{2}$$

where: *T (solvent)* in °C, boiling point of solvent (acetone) [57]; ΔT change in boiling point calculated for acetone; K_b in K·kg/mol ebullioscopic constant for pure acetone, having value 1.67 K·kg/mol [58]; m -molality of a solution, mol/kg, where mol of solute was considered another solvent in mixture (acetic acid or DMF); i, Van't Hoff factor is 1 for all systems. Calculation was performed for mixtures Ac/HAc and Ac/DMF.

(b) Initial surface tension measurements were performed using the pendant drop method, by taking images of pear-shaped drops with a high-speed camera of a device OCA-15 Plus Goniometer (Data Physics, Neurtek Instruments, Eibar, Spain), and using Open Access software named Open Drop [59,60]. On average, 10 measurements were performed per solvent/solvent mixture, while a *t*-test was used to study statistically significant differences for means.

2.3.2. Optical microscopy

The optical profilometer Olympus DSX500 (Olympus Iberia, Barcelona, Spain) was used to study the morphology and roughness of samples. Arithmetic mean roughness R_a over the sample area of 1425 × 1425 μm was measured with a cut-off wavelength λ_c chosen according to standard EN ISO 4288. For calculating the average value and deviation, 10 measurements were performed for each side of all samples.

2.3.3. Scanning electron microscopy

The morphology of CA samples was investigated at higher resolution by scanning electron microscopy (SEM) using a Phillips XL30 microscope at an acceleration voltage of 10 kV. Images were analyzed with open-access ImageJ software. The cross-section of Janus films was prepared for imaging by submerging film into the liquid nitrogen and making a crack in a frozen state and recorded with field emission scanning electron microscope (FESEM) TENEO-FEI. The signal arising from secondary electrons (SE) was used to generate the FESEM images using an acceleration voltage of 10 kV. To avoid electrostatic charge accumulation, the samples used for SEM and FESEM were gold coated by sputtering with Leica EM ACE 200 Sputter coater (current of 30 mA for 40 s).

2.3.4. Differential scanning calorimetry

Differential scanning calorimetry (DSC) was performed using a Mettler Toledo 822e calorimeter, under a nitrogen atmosphere. The thermal program consisted of three steps, first heating scan from 50 to 260 °C at a rate of 10 °C/min, followed by an isothermal measurement at 260 °C for 5 min, then a cooling scan at 10 °C/min, and finally a second heating scan from 50 to 260 °C at 10 °C/min. The crystallinity of samples, χ, is calculated from the first heating scan by dividing the enthalpy of fusion of samples by enthalpy of fusion of 100% crystalline cellulose triacetate, 58.8 J·g^{-1} [61].

2.3.5. Infrared spectroscopy ATR-FTIR

Investigation of a molecular structure was performed using Thermo Fisher Nicolet iS 5 spectrometer coupled with an ATR device with diamond window GladiATR (PIKE Technologies). Samples were measured in a range of 400–4000 cm^{-1} using 32 scans and 2 cm^{-1} resolution.

2.3.6. Contact angle measurements

Contact angle, using water as testing liquid (3 μl volume), was measured by sessile drop method on OCA-15 Plus Goniometer (Data Physics, Neurtek Instruments, Eibar, Spain). Reported values are the average of 4 measurements per sample. Photographs during wetting and corresponding contact angle measurements were taken at 5, 30, 60, 90, and 120 s. For all samples, measurements were performed at both sides (2 measurements per side), while for the double-layered film each side was measured 4 times. For the double-layered film, measurements were extended to 300 s to analyze contact angle evolution over an extended period of time.

2.3.7. Thickness of samples and porosity

Sample thicknesses were measured with Easy-check FN (Neurtek Instruments) with an accuracy of ± 1 μm. The results are presented as mean values of 8 measurements. Porosity was calculated according to the method described in [62]. The weight of films of a known volume (surface area multiplied by thickness), i.e. an apparent density in g/cm^3, ρ_a, is divided by the real density of pure solid CA (taken from the data of the manufacturer, Sigma Aldrich, 1.3 g/cm^3), ρ_0, to estimate the porosity, φ, using the equation (3):

$$\phi = 1 - \frac{\rho_a}{\rho_o} \tag{3}$$

2.3.8. Mechanical tests

Mechanical characterization of the double-layered film was performed using a testing machine Microtest DT/005/FR (Microtest

S.A., Madrid, Spain) with a load cell of 50 N. Samples were tested in a uniaxial tensile configuration using a loading rate of 10 mm/min. The dimensions of the specimens were 40 mm length, 10 mm width, and the gap between the grips of the testing device was set to 20 mm. Mechanical tests were done in triplicate.

3. Results and discussion

3.1. Effect of solvent mixture composition and concentration of corresponding polymer solutions

For the first time, a series of preliminary experiments were conducted to test various combinations of solvents and concentrations (8–16% w/v) of CA concerning the production of CA-based materials by SBS. Up-to-date, Dadol et al. [51] reported successful SBS of composite CA/PAN nanofibers, and CA fibers alongside PEO were also produced with the use of acetic/formic acids as solvent system [63]. Besides, another investigation by El-Newehy and coauthors [64] reported the production of pure CA nanofibers from a 15 wt % solution of CA in acetone. However, several problems were encountered in our configuration when reproducing their work. Low air pressure (0.5 bar) (even though convenient because of the fast evaporation of acetone) in our work led to the deposition of the material at the exit of the nozzle and the blocking of the device. Although the lowest injection rate (0.12 ml/min) was used, high polymer concentration (15 wt%) could not be processed. After a large set of experiments and results, (details in *Supplementary material*) several conclusions can be made, which can be divided in terms of the solvent used to process CA by SBS (pure acetone, mixtures Ac/HAc, and mixtures Ac/DMF).

3.1.1. Solution blow spinning of cellulose acetate using as solvent pure acetone

In consideration of CA solution in acetone, high injection rates (0.5 ml/min) could be used for low-concentrated solutions (less than 12%, Table S1). However, the appearance of the first fibers occurs when the concentration is at least 10% and lots of beads are formed (Fig. S1). This material has an appearance of a thin fragile sheet that breaks when attempted to remove from the collector. At the concentration of 8%, only the collection of a powder on the collector is obtained. An increase of concentration up to 12% requires the reduction of injection rate from 0.5 to 0.25 ml/min. At the same time, due to the high evaporation rate of acetone, air pressure no higher than 1 bar could be used. Also, the distance of the nozzle from the collector plays an important role. Table S1 shows that when using a working distance of 7 cm thin sheet is produced which was very difficult to detach from the collector. However, when the working distance is increased to 10 cm, powder-like sheets form, and upon removal from the collector it breaks. This is a consequence of very fast evaporation that does not allow polymer solution flow, with the corresponding elongation, to produce continuous fibers (Fig. S2). It was not possible to produce any material with a concentration increase beyond 12%. Regardless of combinations of air pressure and injection rates, no stable production of material was possible and the nozzle was blocked during production. For this reason, mixtures of acetone with other solvents of a higher boiling point were prepared and used for solution preparation.

3.1.2. Solution blow spinning of cellulose acetate from a mixture of acetone and acetic acid

To reduce the fast evaporation of acetone as a solvent, acetic acid is added in various proportions. After the required experimental work it can be concluded that the technical limitations of processing CA in a mixture of acetone/acetic acid using an SBS device were 14% of CA concentration and 70% v/v of acetone in the solvent mixture Ac/HAc (Table S2). Multi-structured membranes, although hard to separate from the collector, were produced using these conditions of polymer solution (Fig. S3). In general, 0.25 ml/min was the maximum injection rate that could be used in the Ac/HAc solvent mixture with 12% CA, and, as in the case of pure acetone, an increase of concentration invokes the necessity to reduce the injection rate.

3.1.3. Solution blow spinning of cellulose acetate from a mixture of acetone and DMF

Mixing a high boiling point solvent such as DMF with acetone, enabled easier production of CA material. With DMF in the mixture up to 30% v/v, high processing rates can be achieved, even with relatively high concentrations (14% could be processed with an injection rate of 0.5 ml/min and 16% with 0.25 ml/min). However, high injection rates require high air pressure which might induce too fast evaporation of a solvent and because of too fast evaporation, solid material might be accumulated at the exit of the nozzle inducing clogging. Therefore, as can be seen from Table S3, to get materials in the form of films constituted by, at least, some fibers, when relatively high concentrations are used, low air pressures are required. On the other hand, if air pressure is too low, there is not enough force to stretch the polymer solution to finally yield the expected fibers. This is one of the reasons why, when using these particular solvent mixtures, submicrometric or nanofibers were not formed but films. Using a solvent mixture of Ac/DMF 70:30 ratio, in any concentration of polymer, leads to a formation of a thin film on the collector, whereby thickness can be adjusted by the volume of a processed solution. By slowly decreasing DMF ratio in a mixture from 30% to 10%, as will be presented in the next section, multi-structured membranes constituted by beads and submicrometric fibers were produced.

3.2. Influence of solvent system on morphology of produced materials

To study the influence of the solvent system on the morphology of produced CA materials, 12%, and 14% polymer concentration were chosen with a mixture of Ac/HAc (ratio 70:30) and Ac/DMF (ratios 70:30, 80:20, 90:10). All processing parameters during SBS were kept constant (working distance = 15 cm, air pressure at the nozzle exit = 1 bar, rotational speed of the collector = 52 RPM), and for 12% concentration of polymer solution, 0.25 ml/min injection rate was used, while for 14% 0.125 ml/min was used. In Fig. 2(a-c) SEM images of the materials are shown where a morphology mainly constituted by corpuscles and submicrometric fibers can be observed. After careful image analysis average diameter of submicrometric fibers was obtained (Fig. 2d,e). The shortest diameters with also the lowest deviations were found in the samples produced from 12% CA solutions using Ac/HAc (70:30) and Ac/DMF (90:10) solvent mixtures, having average diameters of 843 ± 268 nm and 683 ± 193 nm, respectively. However, these submicrometric fibers are frequently connected through lumps and the beads are dominant morphological structures. It was tested whether an increase of rotational speed up to 250 RPM changes thequality, orientation, and diameter of submicrometric fibers, however, no improvement was observed. For further investigation, a rotational speed of 250 RPM and a concentration of 12% of CA were chosen, since this concentration enabled the use of a higher injection rate (0.25 ml/min), which can be of practical significance for potential industrial scale-up.

Flat films on the collector were obtained only in the case of using Ac/DMF solvent mixture in a ratio of 70:30. As can be seen in Fig. 3 these films have a corpuscular morphology, which is probably formed, upon drying on the collector, from coalescent droplets. One possible reason for droplet formation is an increase of

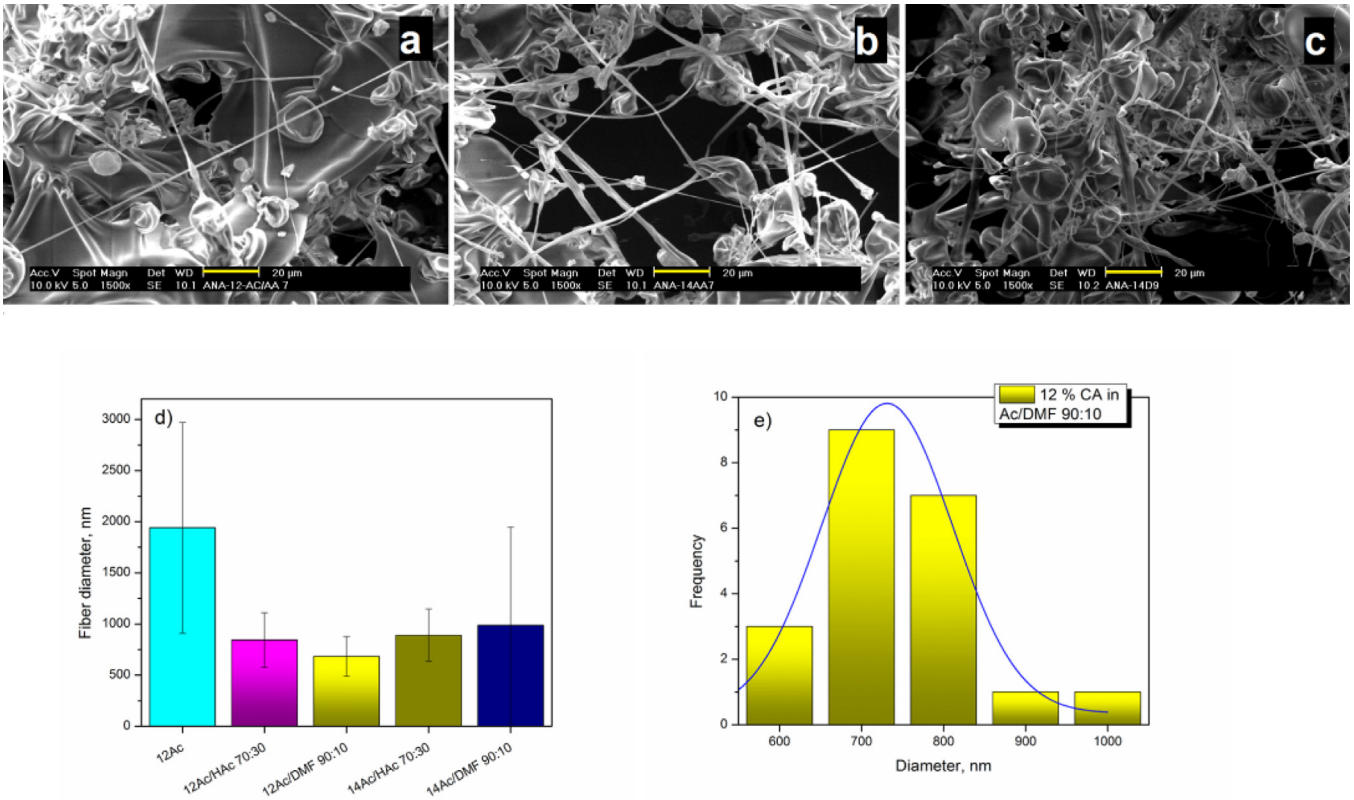

Fig. 2. SEM images of CA materials produced using different concentrations: a) 12% Ac/Hac 70:30, b) 14% Ac/Hac 70:30, c) 14% Ac/DMF 90:10, d) fiber mean diameters obtained from SBS of CA in various solvent systems and e) distribution of fibers size produced from 12% CA solution in solvent mixture Ac/DMF 90:10, given as an example. (yellow scale bar size is 20 μm). (For interpretation of the references to colour in this figure legend, the reader is referred to the web version of this article.)

boiling point when DMF is included in the solvent mixture, lowering the evaporation rate (Table 1). With a further decrease of DMF in the mixture, a transition of morphology from pure beads to beads with submicrometric fibers is observed (Fig. 3). Samples produced from a solution prepared with solvent mixtures of Ac/HAc (Fig. 2a) and Ac/DMF (Fig. 3 third column), with the same ratio of solvents (70:30), are clearly different. A multi-structured membrane is obtained in the case of using Ac/HAc, while a film is obtained when DMF is in a mixture. To elucidate this, several aspects need to be taken into consideration. The most frequent argument for fibers production failure in electrospinning is a lack of sufficient concentration for chain entanglement [65]. This is frequently linked to the viscosity of polymer solution since higher viscosity is associated with a smaller distance between macromolecular chains in a solution, enough to induce entanglement and consequently the formation of fibers [65].

In SBS, a very important parameter seems to be the boiling point i.e. evaporation rate and surface tension of solvent since pressurized air is the driving force for fibers formation, allowing elongation of the polymer solution and evaporation of the solvent. At 12% concentration of CA, using only acetone as a solvent, submicrometric fibers were formed but, due to solution properties, SBS is frequently interrupted by nozzle clogging even with very low injection rates of 0.12 ml/min. The addition of a higher boiling point solvent to acetone, acetic acid, or DMF, resulted in the production of materials without interruptions, enabling higher injection rates, obtaining multi-structured membranes when using acetic acid and flat films in the case of using DMF. In this case, surface tension can be assumed as the main factor influencing the final morphology obtained. Surface tensions for the solutions Ac/HAc 70:30 and Ac/DMF 90:10 (for which CA solutions processed by SBS in this work gave fibrous morphology) are lower than the surface tension obtained for Ac/DMF 70:30 that induced film formation (Table 1). Therefore, it seems that submicrometric fibers can be obtained only when applied pressurized air can overcome the surface tension of polymer solution, to elongate it and thus facilitate the formation of fibers. Morphology constituted by beads can be obtained by electrospinning as well when solvent mixtures of acetone and DMF contains a higher relative amount of DMF as shown by Lee et al. [5]. Increase of CA concentration and/or decrease in DMF ratio, fibers with beads or even beadles fibers can be obtained [5]. In our case, regardless of the Ac/DMF ratio, nanofibers or submicrometric fibers free of beads could not be obtained even with high concentrations of polymer in solution, 14% and 16%. From Fig. 2d can be concluded that an increase of concentration to 14% of CA in Ac/DMF 90:10 allows producing more submicrometric fibers but with higher diameters and higher deviation from a mean value. Nevertheless, the complex morphology of materials obtained in this work will prove to be beneficial for hydrophobic behavior, which will be presented further in the article.

3.3. Crystallinity and thermal behavior of produced CA materials

The solvent system used for a solution blow spinning of CA materials can affect their structure as well as their thermal properties and crystallinity. DSC traces obtained in the first heating scan (Fig. 4a) show that the glass transition temperature (T_g) of materials depends on the solvent system used during SBS. The lowest T_g is measured in the sample produced from Ac/HAc 70:30 and the highest one in the sample produced from Ac/DMF 90:10, having values of 190 °C and 202 °C respectively. The small sharp shoulder peak in a sample prepared from Ac/DMF 80:20 (at ~ 170 °C) is considered, due to its shape and size, as an artifact [66]. These materi-

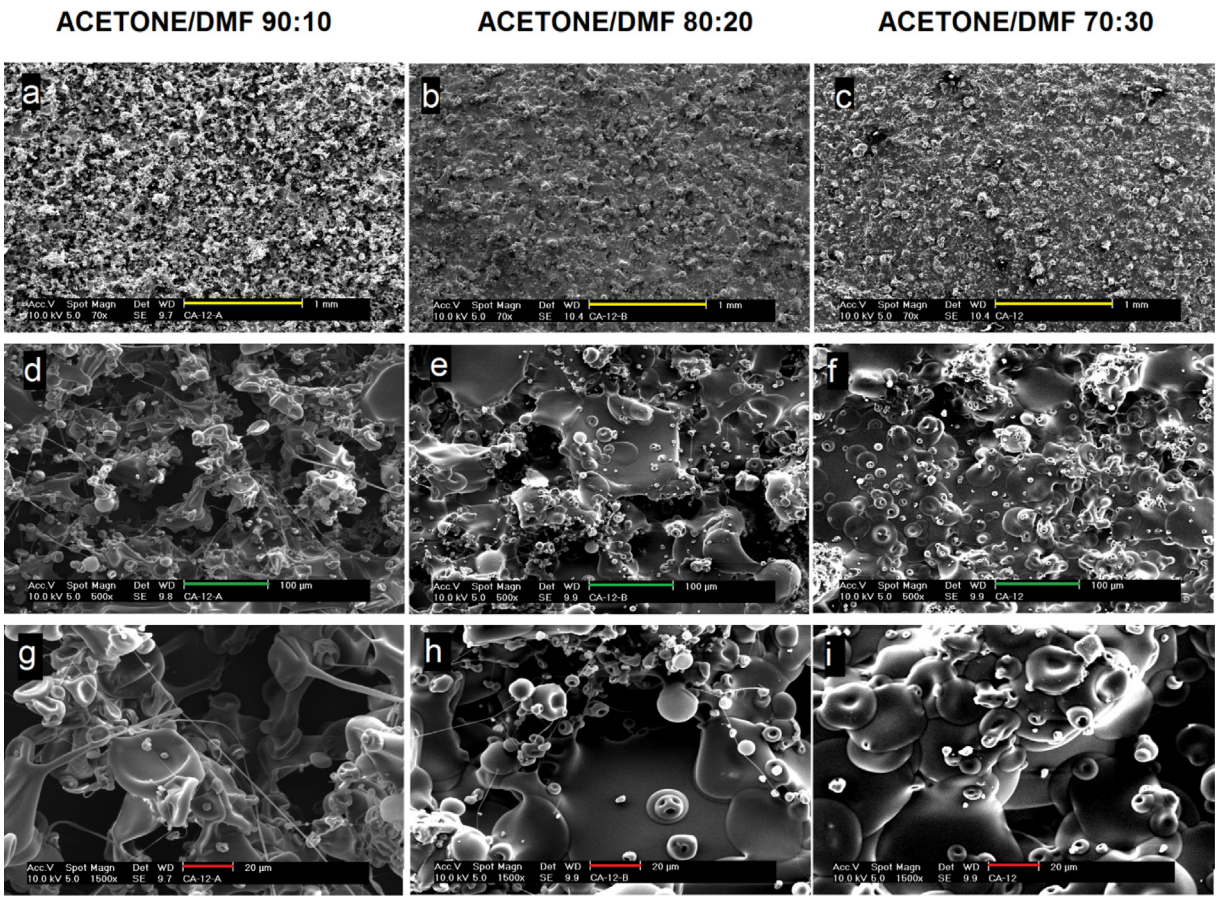

Fig. 3. SEM images of CA produced from various solvent systems of the 12% concentration, using injection rate 0.25 ml/min, air pressure 1 bar, distance of the nozzle from the collector 15 cm, rotational speed of the collector 250 RPM (a,b,c-yellow scale bar size 1 mm; d,e,f-green scale bar size 100 μm; g,h,i-red scale bar size 20 μm). (For interpretation of the references to colour in this figure legend, the reader is referred to the web version of this article.)

Table 1
Some physical properties of solution mixtures used in this work.

Solvent	Boiling point (°C)	Surface tension (mN/m)	Density (g/cm^3)
Acetone	56	23.3 ± 0.18	0.7627
Ac/DMF 90:10	59	24.2 ± 0.08	0.7776
Ac/DMF 70:30	68	25.8 ± 0.54	0.8064
Ac/HAc 70:30	72	24.9 ± 0.17	0.8551

als are multi-structured membranes constituted by fibers and beads. Peaks of melting temperature for these two samples are almost identical (225.3 °C and 225.9 °C) and very similar to other reported values [2,67,68]. Besides, the same values of enthalpy of fusion were obtained as well as the corresponding calculated crystallinity (Fig. 4b). These results suggest that crystallinity fraction is not the reason for the differences observed in the T_g's. On the other hand, the highest crystallinity and the highest melting temperature were obtained in the film produced using solution blow spinning with Ac/DMF 70:30 solvent mixture. The lowest crystallinity and therefore, the most amorphous material was found in multi-structured membranes produced from the lowest amount of DMF in the mixture (Ac/DMF 90:10) and also from the mixture containing acetone with acetic acid.

When only solution mixtures of acetone with DMF are considered, it can be noted that a decrease in the relative amount of DMF leads to a decrease of crystallinity and a decrease in the melting temperature of materials, together with an increase in glass transition temperature. In other words, even though a low relative amount of DMF induced the formation of some fibrous morphology, it causes a higher fraction of amorphous phase with less mobility. Similarly to this, it has already been shown that in the case of ES, in general, less crystalline materials can be obtained although constituted by nanofibers with an orientation of the macromolecules along the fiber axis [69]. This is explained by the fact that the rapid formation of fibers (stretching and solidification) during ES does not allow crystal formation, but there exists some orientation of macromolecules. In our work, this could be a possible reason for higher T_g but lower T_m peak. During the production of multi-structured membranes, fewer crystalline regions in fibers are formed but the macromolecular orientation can be more adequate to enhance intermolecular interactions which may result in lower chain mobility and consequently higher glass transition temperature. This is somewhat expected since high pressurized air at the exit of the nozzle during solution blow spinning must cause fast solidification during fibrous or multi-structured membranes formation directly from the polymer solution, facilitating the production of amorphous material.

3.4. Roughness, wettability, thickness, and porosity of produced materials

Different morphologies, as stated in Introduction, can affect the wettability of materials, therefore in this work wettability was studied using contact angle measurements. It was found that fibrous-like membrane produced from a mixture of solvents Ac/DMF 90:10 has high water contact angles exhibiting hydrophobic behavior (Table 2). From the observation of the morphology of

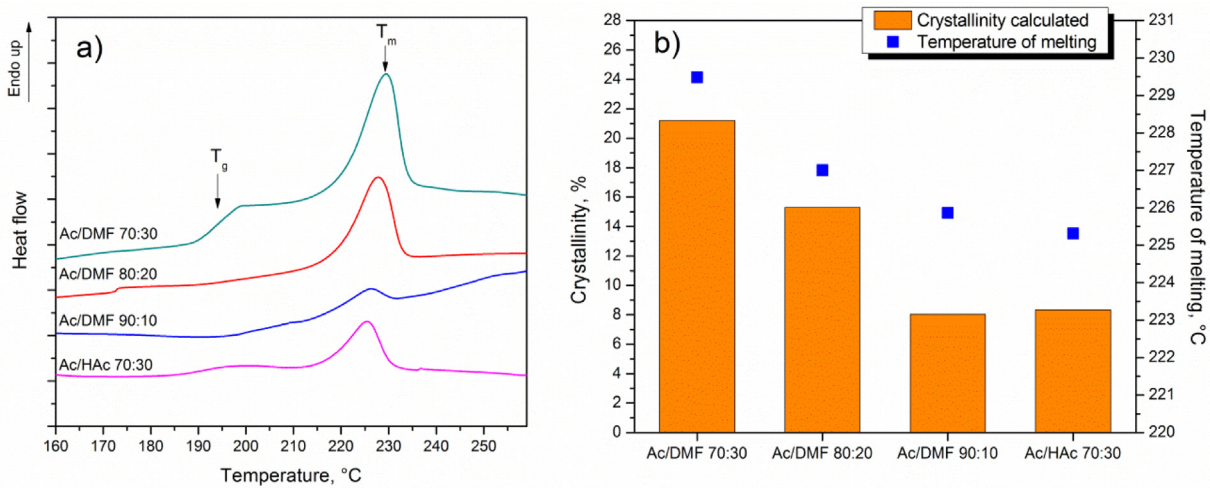

Fig. 4. a) DSC traces of CA materials prepared in SBS with the use of different solvent systems ; b) crystallinity calculated from enthalpy of melting and peaks of melting temperatures for cellulose acetate prepared from different solvent mixtures.

Table 2
Measured contact angles of samples after 5 s and 120 s of the water drop deposition.

Sample	Contact angle (°) after 5 sec	Contact angle (°) after 120 sec
Ac/HAc 70:30	81.9 ± 3	77.2 ± 3.1
Ac/DMF 70:30	69.8 ± 3	63.6 ± 6.9
Ac/DMF 80:20	89 ± 3	85.2 ± 2.7
Ac/DMF 90:10	104 ± 5	97.4 ± 2

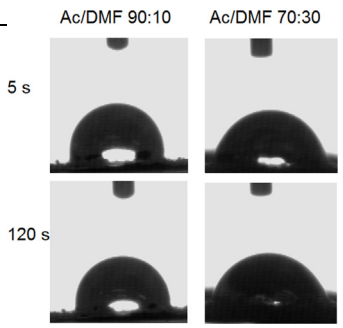

CA multi-structured materials produced from a solvent system containing Ac/HAc 70:30 and Ac/DMF 90:10 (Fig. 5) one would expect similar values of contact angle. However, as can be seen in Table 2, the contact angle of CA produced from Ac/HAc (70:30) is lower than for the corresponding fibrous material obtained from Ac/DMF (90:10).

This can be related to the fact that higher roughness of the surface can induce more hydrophobic behavior. In fact, for the materials under study, the higher the roughness the higher the water contact angle. Roughness parameter R_a of materials produced from solvents Ac/DMF 90:10 and Ac/HAc 70:30 is 17.2 ± 4 μm and 11.5 ± 3 μm, respectively.

Furthermore, for the samples produced from different relative amount of DMF in the solvent mixtures Ac/DMF, there is a morphology transition from films to multi-structured membranes which is in line with the roughness and water contact angle evolutions (Fig. 3 and Fig. 6). When average roughness increases, water contact angle also increases (Fig. 6a). Besides, as expected, the same trend can be noted for porosity and thickness of this set of samples (Fig. 6b).

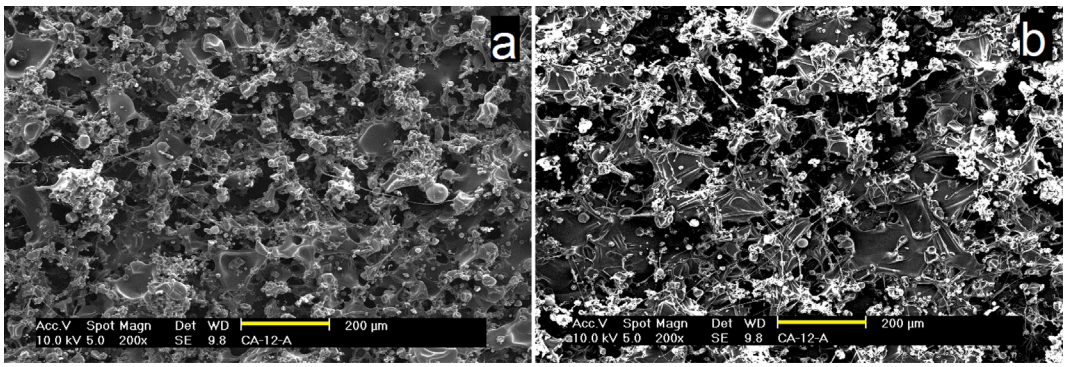

Fig. 5. SEM microphotographs of cellulose acetate materials produced from 12% solutions made with different solvent systems: a) Ac/DMF 90:10, b) Ac/HAc 70:30. (yellow scale bar is 200 μm size). (For interpretation of the references to colour in this figure legend, the reader is referred to the web version of this article.)

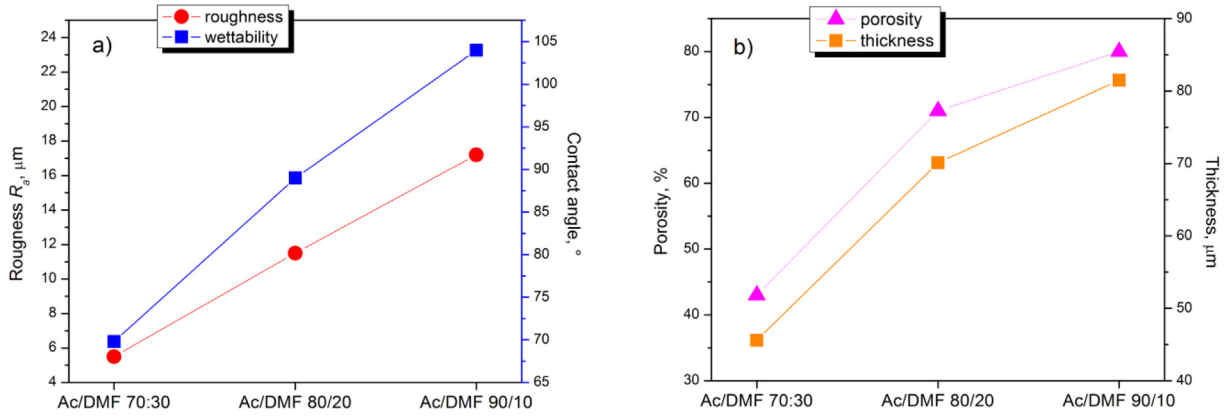

Fig. 6. a) Roughness R_a, contact angle and b) porosity, thickness as a function of solvent mixture used for preparation of spinning solutions of cellulose acetate.

This allows concluding that for obtaining hydrophobic CA using SBS, the existence of beads and corpuscular morphology is beneficial since it can contribute to the formation of the complex morphology required to decrease wettability [70]. With these complex morphologies and the existence of many voids and air pockets, increased hydrophobic behavior is expected [44]. Therefore, the increase of porosity and thickness of prepared CA materials should be indicative of the existence of many voids and air pockets which all together lead to the increase of contact angle as observed, pointing to the Cassie-Baxter model [62] as the best one to explain this wettability behavior. This conclusion is in accordance with the study made by Kasiri et al. [42] where polystyrene prepared by solution blow spinning exhibited very high contact angles, which were explained by the presence of submicrometric fibers in the material and by the heterogeneity of the surface. In the case of electrospun materials, it was already reported that the highly porous material, and the existence of beads and protuberant structures can increase hydrophobicity [44,71]. In our work, from Fig. 6, it is clear that increased surface roughness, coupled with surface heterogeneity (existence of droplet-like structure, fibers and beads) and higher porosity, as it happens in the sample spun from 12% CA in Ac/DMF 90:10, enhances hydrophobicity. Therefore, to obtain hydrophobic material from hydrophilic polymer, so-called beads on a string morphology [72] or complex heterogeneity with high porosity and increased surface roughness [42,44] within a certain range at the microscale, are desirable features. The highest contact angle was measured in the sample Ac/DMF 90:10, exceeding 100°. However, this membrane is fragile due to high porosity and difficult to detach from the aluminum foil which is used to cover the collector. To explore a real possibility for this material to be usable, it would be necessary to prepare it with enough integrity; therefore, a double-layered material was prepared, where a first layer was produced as a thin flat film that serves as a supporting layer and the second layer contains fibrous hydrophobic membrane.

3.5. Preparation of double-layered cellulose acetate film from different solvent mixtures using layer-by-layer SBS processing

The double-layered (DL) film was prepared with the SBS by the sequential processing of an equal amount of two polymer solutions under identical conditions without stopping the machine. A change of syringe filled with polymer solution occurred at the end of the first layer production. The first layer was processed using a solution of 12% CA in Ac/DMF 70:30 and the second layer was subsequently deposited over the first one using a 12% of AC solution in Ac/DMF 90:10. The total production time for both layers took approx. 35 min, for a total volume of 8 ml (4 ml + 4 ml). The individual layers, for comparison in terms of thickness and porosity, were produced using the same amount of a solution in a syringe, 8 ml. The thickness of the double layer has a value between the thicknesses of the individual layers when they are prepared from 8 ml of solution (Table S4). The wettability i.e. contact angle on the top layer of the film (Ac/DMF 90:10) was slightly lower than that observed on the individual film processed using the same solvent system (Fig. 7). The properties of each side, when they are prepared individually, remain in the corresponding side of the double-layered material, exhibiting unique and distinctively different values. The wettability of a top side (TS) is low, with a contact angle of around 95°, while the bottom side (BS) has a contact angle of around 68°. This can qualify the produced film as a Janus-type of film (Fig. 7). Wettability of DL film was further studied up to 300 s, to evaluate the decrease of contact angle after an extended period . Results revealed that for the DL top side contact angle slowly decreases from the average of 95° at the beginning of the measurement, to 85° measured after 5 min. DL bottom side of the film from the starting 68° has a contact angle of 59° after 5 min. This shows that both sides of films have the same steady kinetics of wettability decrease over time and that contact angle decreases at almost the same rate on both sides. Furthermore, porosity and crystallinity calculated from DSC measurements, have values that are in a range between values obtained for individual films (Table S4), while roughness and contact angles of each side adopted values like those of the individual layers. It is important to point out there are small differences between R_a values of individual sides in individual layers too, i.e. differences in the roughness of the side close to the collector during production (bottom side- 70:30 BS) compared to the DL BS and side exposed to air of individual sample (top side- 90:10 TS) compared to the DL TS (Fig. 7). Considering the relation between the roughness and contact angle it can be seen that when surface roughness increases its standard deviation also increases and the contact angle increases. This result reinforces the hypothesis that not only the value of surface roughness contributes to the hydrophobic effect, but also the heterogeneity of the surface which is reflected through a higher standard deviation of the mean roughness. It can be concluded that prepared CA materials, the specific top side of the double-layered film and multi-structured membrane prepared using Ac/DMF in a ratio of 90:10, follow the Cassie-Baxter model during wetting [62], since both materials' surface roughness, porosity, and thickness are high which implies the existence of air pockets below the drop during wetting, reducing, therefore, contact between materials' surface and water.

As it was mentioned in the *Introduction*, some studies about obtaining hydrophobic CA electrospun mats [29,30] suggest that besides roughness and fibrous morphology, a partial contribution

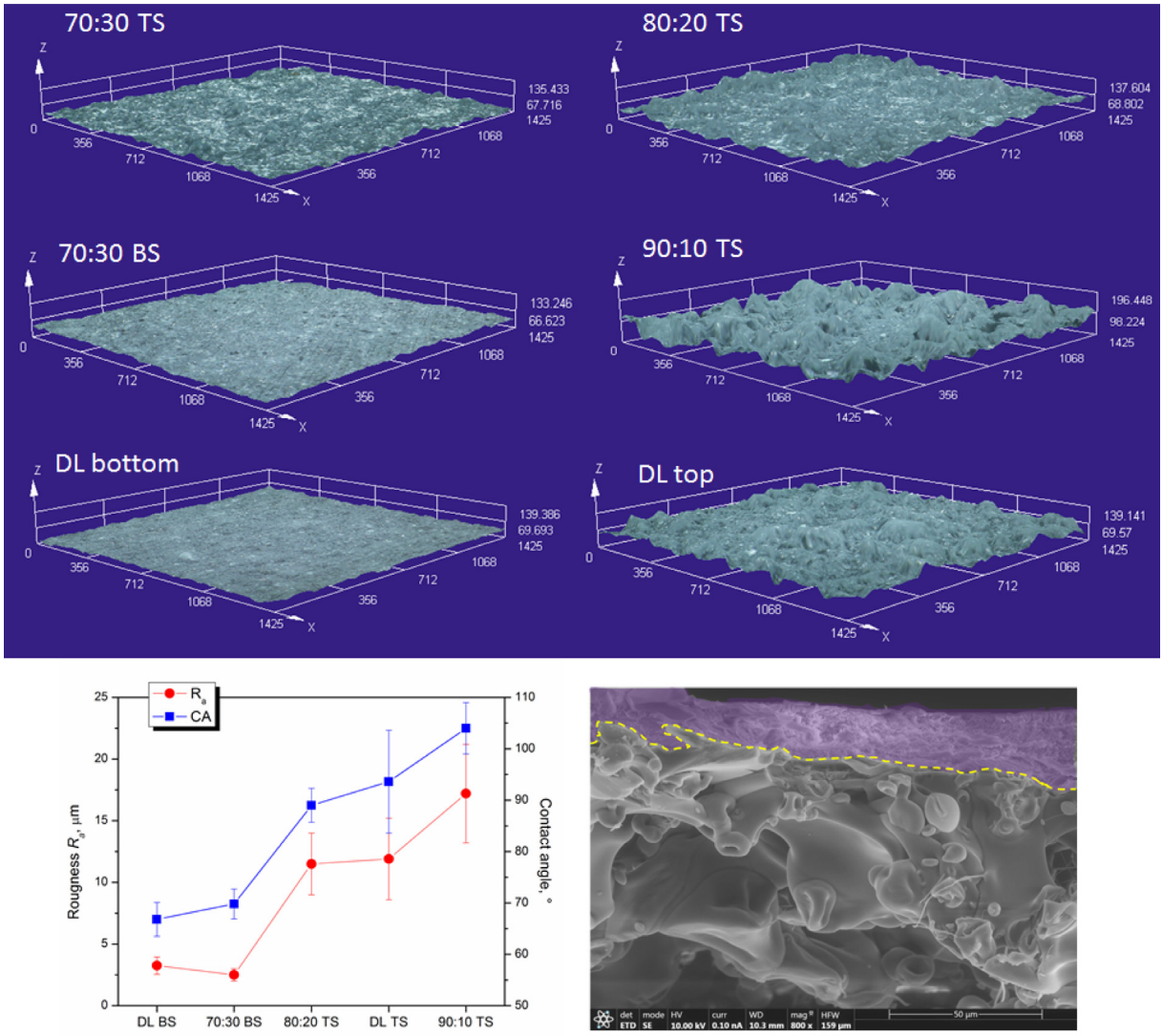

Fig. 7. 3D images obtained from optical profilometer of differently produced cellulose acetate using SBS; TS-top side, BS-bottom side, DL-double layer; 70:30, 80:20 and 90:10 are ratios of acetone and DMF in solutions for SBS; graph represents a roughness parameter R_a and contact angle of different materials; FESEM image represents cross section of double-layered film.

to hydrophobic behavior comes from a different orientation of polar hydroxyl (OH) groups in electrospun CA, which are still present to some extent in acetylated cellulose. In a work by Mikaeili and Gouma [30] this indeed is the case since they have shown, using ATR-FTIR, a clear decrease of the band corresponding to OH groups at 3411 cm^{-1} in the spun CA mats compared to the cast films. In our work, ATR-FTIR analysis (Fig. S4) showed that there is not any significant difference in terms of signal intensity of the OH groups neither on the different sides of the double-layered film nor when comparing individual films (obtained using a mixture of Ac/DMF 70:30) with multi-structured membranes (obtained using mixture Ac/DMF 90:10). Spectra were normalized to the peak with the highest intensity at 1030 cm^{-1}. This peak can be assigned to symmetric C-O-C stretching of the cellulose [73]. The distinctive peak at 1214 cm^{-1} can also be seen corresponding to antisymmetric C-O-C stretching of the ester groups [23]. The peak at 1366 cm^{-1} corresponds to symmetric CH_3 bending. A strong peak at 1735 cm^{-1} corresponds to the carbonyl group stretching [73,74], as expected for CA, while a low-intensity band at 3475 cm^{-1} can be assigned to OH groups. While this particular band showed a distinctive difference in work by Mikaeili and Gouma [30], in our work there is no substantial change in this region; however, a change in intensity of a peak corresponding to carbonyl stretching at 1735 cm^{-1} was found (Table 3). According to these results, it can be concluded that in CA materials produced using a solvent mixture with a lower amount of DMF (Ac/DMF 90:10) the higher content of acetyl groups exist on the surface thus promoting increased hydrophobic effect compared to CA produced with a higher relative amount of DMF (Ac/DMF 70:30) since acetyl groups with carbonyl moiety are less hydrophilic than non-

Table 3
Intensity and area of a band centered at 1735 cm^{-1} and assigned to the -C = O stretching in the acetyl groups of CA.

Sample	Intensity of a band at 1735 cm^{-1}	Area of a band at 1735 cm^{-1}
DL top side	0.63	26.3
DL bottom side	0.50	20.3
IL 70:30 bottom side	0.49	20.9
IL 90:10	0.62	25.9

esterified hydroxyl groups. It is important to highlight here that preservation of this particular molecular orientation of acetyl groups enabled that double-layered film maintained in each side wettability behavior of the corresponding individual layer.

Results presented here are significant because they show that it is possible to choose and design properties of double-layered film produced by solution blow spinning based on the properties of individual layers; this opens up a potential novel approach for obtaining films with distinctively different sides i.e. Janus films. Janus films are very attractive materials that per definition have two distinctively different sides, with contradicting properties, the most important being wettability [75]. When considering polymeric membranes, the Janus membrane is prepared usually from two different polymers [75] and our work here clearly shows the advantage of design and preparation of a Janus-like membrane from the same polymer, without additional chemical modification of the surface. Since two layers in the presented study have approx. 30° difference in wettability and the top side has 3.6 times higher average surface roughness, future work will aim at a variation of the ratio and thickness of individual layers to enhance the difference and improve the final properties of the resulting double-layered film.

For various applications, the mechanical properties are also important; therefore we tested the mechanical properties of DL film. The maximum breaking strength of 13.5 ± 2.25 MPa, elongation at break of 12.9 ± 3 mm, and elastic modulus of 181.4 ± 32.2 MPa were measured. The representative stress–strain curves are given in Fig. S5 (Supplementary material). The mechanical properties of produced materials in this work are comparable to other reported CA electrospun membranes [76,77]. The future studies will aim at expanding the analysis of mechanical properties of the double-layered cellulose acetate material as a function of different ratios of layers.

4. Conclusion

Cellulose acetate materials (CA), as renewable and biodegradable, are gaining increased interest in previous years for many applications. For some applications such as food packaging, the hydrophilicity of CA is an obstacle that can be addressed by different production methods, such as electrospinning as shown by other authors, or solution blow spinning (SBS) as shown here in this work. Extensive research into the processing of CA using SBS as a technique for a multi-structured membrane consisting of submicrometric fibers with beads and film preparation is presented since it is known that wettability is highly dependent on the morphology of produced material. Various solvents, acetone, acetic acid, and DMF, were used for the preparation of CA solutions. We have shown that morphology and wettability are highly dependent on the solvent system used for polymer solution while keeping all other SBS parameters constant. Multi-structured morphology with many beads, submicrometric fibers, and accumulated material, can be obtained by spinning CA from a solution containing a relatively low amount of DMF in acetone (10%); an increase of DMF up to 30% results in the hydrophilic flat film formed on a collector. Sequential deposition of different solutions of CA offers the possibility to produce two-sided films, with distinctive differences in wettability, having one side hydrophilic and the other hydrophobic, as well as the difference in crystallinity and surface roughness. Each side of the resulting film has adopted properties of individual layers from which it was assembled; therefore offering the possibility to design desired properties of each side by knowing the properties of individual layers. We consider this a significant advantage of the SBS technique and hope to inspire more work in the field of preparation of Janus membrane from the same polymer, without the need for chemical modification of one or both sides. In addition to the advantage of being a very robust method, with SBS used in this work, a high processing rate can be achieved, which makes it a promising technique for industrial scale-up.

CRediT authorship contribution statement

Ana Kramar: Conceptualization, Methodology, Formal analysis, Investigation, Visualization, Writing – original draft, Funding acquisition. **Javier González-Benito:** Validation, Visualization, Supervision, Writing – review & editing, Funding acquisition.

Data availability

Data will be made available on request.

Declaration of Competing Interest

The authors declare that they have no known competing financial interests or personal relationships that could have appeared to influence the work reported in this paper.

Acknowledgement

The authors would like to thank Irene Rodriguez Ortega, MSc, for technical support, help during the solution blow spinning of materials presented in this work, and for the graphical illustration of the SBS device given in Fig. 1 and in the graphical abstract.

Funding

This work was financially supported by CONEX-Plus program of Universidad Carlos III de Madrid (UC3M) and the European Commission through the Marie-Sklodowska Curie COFUND Action (Grant Agreement No 801538). Authors also appreciate the financial support received from AEI, The Ministry of Science and Innovation of Spain [PID2020-112713RB-C22 and –C21], Universidad Carlos III de Madrid, Funds for Investigation of Fco. Javier González Benito [2012/00130/004] and the strategic Action in Multifunctional Nanocomposite Materials [2011/00287/003].

Data availability

All additional data will be made available on request.

Appendix A. Supplementary data

Supplementary data to this article can be found online at https://doi.org/10.1016/j.matdes.2023.111788.

References

[1] D. Klemm, B. Philipp, T. Heinze, U. Heinze, W. Wagenknecht, Comprehensive Cellulose Chemistry; Volume l: Fundamentals and Analytical Methods, Wiley-VCH, 1998.
[2] P. Zugenmaier, Crystalline cellulose and derivatives- Characterization and structures, Springer-Verlag Berlin Heidelberg, 2008.
[3] L. Menachem, ed., Handbook of fiber chemistry, CRC Press Taylor& Francis Group, 2007.
[4] K.J. Edgar, C.M. Buchanan, J.S. Debenham, P.A. Rundquist, B.D. Seiler, M.C. Shelton, D. Tindall, Advances in cellulose ester performance and applicaton, Prog. Polym. Sci. 26 (2001) 1605–1688, https://doi.org/10.1016/S0079-6700(01)00027-2.
[5] H. Lee, M. Nishino, D. Sohn, J.S. Lee, I.S. Kim, Control of the morphology of cellulose acetate nanofibers via electrospinning, Cellulose 25 (2018) 2829–2837, https://doi.org/10.1007/s10570-018-1744-0.
[6] E.A. Al Matroushi, Y.E. Greish, M.A. Meetani, B.A. Al Shamisi, Application of cellulose acetate fibrous membranes in the removal of micro- and submicron

solid particulates in drinking water media, Desalin., Water Treat. 57 (2016) 15676–15686, https://doi.org/10.1080/19443994.2015.1131199.
[7] H. Liu, Y. Lo Hsieh, Ultrafine fibrous cellulose membranes from electrospinning of cellulose acetate, J. Polym. Sci. Part B Polym. Phys. 40 (2002) 2119–2129, https://doi.org/10.1002/polb.10261.
[8] A. Kumar, S. Sinha-Ray, A review on biopolymer-based fibers via electrospinning and solution blowing and their applications, Fibers. 6 (2018) 1–53, https://doi.org/10.3390/fib6030045.
[9] H.S. Sofi, T. Akram, N. Shabir, R. Vasita, A.H. Jadhav, F.A. Sheikh, Regenerated cellulose nanofibers from cellulose acetate: Incorporating hydroxyapatite (HAp) and silver (Ag) nanoparticles (NPs), as a scaffold for tissue engineering applications, Mater. Sci. Eng. C. 118 (2021), https://doi.org/10.1016/j.msec.2020.111547 111547.
[10] H.M. Mousa, K.H. Hussein, M.M. Sayed, M.K. Abd El-Rahman, H.M. Woo, Development and characterization of cellulose/iron acetate nanofibers for bone tissue engineering applications, Polymers 13 (2021) 1–17, https://doi.org/10.3390/polym13081339.
[11] R.T. Thomas, J.I. Del Río, K. de Vicente, M. Zhang, H. Karzarjeddi, K.O. Liimatainen, Size exclusion and affinity-based removal of nanoparticles with electrospun cellulose acetate membranes infused with functionalized cellulose nanocrystals, Mater. Des. 217 (2022), https://doi.org/10.1016/j.matdes.2022.110654 110654.
[12] C. Wang, Y. Zhan, Y. Wu, X. Shi, Y. Du, Y. Luo, H. Deng, TiO2/rectorite-trapped cellulose composite nanofibrous mats for multiple heavy metal adsorption, Int. J. Biol. Macromol. 183 (2021) 245–253, https://doi.org/10.1016/j.ijbiomac.2021.04.085.
[13] A. Ojstršek, D. Fakin, S. Hribernik, T. Fakin, M. Bračič, M. Kurečič, Electrospun nanofibrous composites from cellulose acetate / ultra-high silica zeolites and their potential for VOC adsorption from air, Carbohydr. Polym. 236 (2020), https://doi.org/10.1016/j.carbpol.2020.116071.
[14] T.I. Shalaby, M.F. El-Kady, A.E.H.M. Zaki, S.M. El-Kholy, Preparation and application of magnetite nanoparticles immobilized on cellulose acetate nanofibers for lead removal from polluted water, Water Sci. Technol, Water Supply 17 (2017) 176–187, https://doi.org/10.2166/ws.2016.124.
[15] A. Li, Z. Han, Z. Li, J. Li, X. Li, Z. Zhang, A PTHrP-2 loaded adhesive cellulose acetate nanofiber mat as wound dressing accelerates wound healing, Mater. Des. 212 (2021), https://doi.org/10.1016/j.matdes.2021.110241 110241.
[16] A.G.B. Pereira, A.R. Fajardo, A.P. Gerola, J.H.S. Rodrigues, C.V. Nakamura, E.C. Muniz, Y. Lo Hsieh, First report of electrospun cellulose acetate nanofibers mats with chitin and chitosan nanowhiskers: Fabrication, characterization, and antibacterial activity, Carbohydr. Polym. 250 (2020), https://doi.org/10.1016/j.carbpol.2020.116954.
[17] L. Jia, X. Huang, H. Liang, Q. Tao, Enhanced hydrophilic and antibacterial efficiencies by the synergetic effect TiO2 nanofiber and graphene oxide in cellulose acetate nanofibers, Int. J. Biol. Macromol. 132 (2019) 1039–1043, https://doi.org/10.1016/j.ijbiomac.2019.03.204.
[18] E. Vatankhah, Rosmarinic acid-loaded electrospun nanofibers: In vitro release kinetic study and bioactivity assessment, Eng. Life Sci. 18 (2018) 732–742, https://doi.org/10.1002/elsc.201800046.
[19] A. Rezaei, A. Nasirpour, M. Fathi, Application of cellulosic nanofibers in food science using electrospinning and its potential risk, Compr. Rev. Food Sci. Food Saf. 14 (2015) 269–284, https://doi.org/10.1111/1541-4337.12128.
[20] J. Xie, Y.C. Hung, Methodology to evaluate the antimicrobial effectiveness of UV-activated TiO2 nanoparticle-embedded cellulose acetate film, Food Control 106 (2019), https://doi.org/10.1016/j.foodcont.2019.06.016.
[21] F.J. Rodríguez, R.L. Abarca, J.E. Bruna, P.E. Moya, M.J. Galotto, A. Guarda, M. Padula, Effect of organoclay and preparation method on properties of antimicrobial cellulose acetate films, Polym. Compos. 40 (2019) 2311–2319, https://doi.org/10.1002/pc.25041.
[22] P.J.P. Espitia, N.D.F.F. Soares, L.C.M. Botti, W.A. Silva, Effect of essential oils in the properties of cellulosic active packaging, Macromol. Symp. 299–300 (2011) 199–205, https://doi.org/10.1002/masy.200900124.
[23] S.M. Gonçalves, D.C. dos Santos, J.F.G. Motta, R.R. dos Santos, D.W.H. Chávez, N. R. de Melo, Structure and functional properties of cellulose acetate films incorporated with glycerol, Carbohydr. Polym. 209 (2019) 190–197, https://doi.org/10.1016/j.carbpol.2019.01.031.
[24] M. Do Socorro Rocha Bastos, L. Da Silva Laurentino, K.M. Canuto, L.G. Mendes, C.M. Martins, S.M.F. Silva, R.F. Furtado, S. Kim, A. Biswas, H.N. Cheng, Physical and mechanical testing of essential oil-embedded cellulose ester films, Polym. Test. 49 (2016) 156–161. https://doi.org/10.1016/j.polymertesting.2015.11.006.
[25] K. Harini, M. Sukumar, Development of cellulose-based migratory and nonmigratory active packaging films, Carbohydr. Polym. 204 (2019) 202–213, https://doi.org/10.1016/j.carbpol.2018.10.018.
[26] J. Vartiainen, M. Vähä-Nissi, A. Harlin, Biopolymer Films and Coatings in Packaging Applications—A Review of Recent Developments, Mater. Sci. Appl. 05 (2014) 708–718, https://doi.org/10.4236/msa.2014.510072.
[27] G.L. Robertson, Legislative and Safety Aspects of Food Packaging, 2020. https://doi.org/10.1201/b21347-27.
[28] X. Zhou, X. Lin, K.L. White, S. Lin, H. Wu, S. Cao, L. Huang, L. Chen, Effect of the degree of substitution on the hydrophobicity of acetylated cellulose for production of liquid marbles, Cellul. 23 (2016) 811–821, https://doi.org/10.1007/s10570-015-0856-z.
[29] S. Wu, X. Qin, M. Li, The structure and properties of cellulose acetate materials: A comparative study on electrospun membranes and casted films, J. Ind. Text. 44 (2014) 85–98, https://doi.org/10.1177/1528083713477443.
[30] F. Mikaeili, P.I. Gouma, Super Water-Repellent Cellulose Acetate Mats, Sci. Rep. 8 (2018) 1–8, https://doi.org/10.1038/s41598-018-30693-2.
[31] A. Ruhela, G.N. Kasinathan, S.N. Rath, M. Sasikala, C.S. Sharma, Electrospun freestanding hydrophobic fabric as a potential polymer semi-permeable membrane for islet encapsulation, Mater. Sci. Eng. C. 118 (2021), https://doi.org/10.1016/j.msec.2020.111409 111409.
[32] H. Liu, C. Tang, Electrospinning of cellulose acetate in solvent mixture N, N-dimethylacetamide (DMAc)/acetone, Polym. J. 39 (2007) 65–72, https://doi.org/10.1295/polymj.PJ2006117.
[33] E.S. Medeiros, G.M. Glenn, A.P. Klamczynski, W.J. Orts, L.H.C. Mattoso, Solution blow spinning: A new method to produce Micro- and Nanofibers from Polymer solutions, J. Appl. Polym. Sci. 113 (2009) 2322–2330, https://doi.org/10.1002/app.
[34] M. Rotta, M. Motta, A.L. Pessoa, C.L. Carvalho, W.A. Ortiz, R. Zadorosny, Solution blow spinning control of morphology and production rate of complex superconducting YBa 2 Cu 3 O 7–x nanowires, J. Mater. Sci. Mater. Electron. 30 (2019) 9045–9050, https://doi.org/10.1007/s10854-019-01236-w.
[35] E.S. Medeiros, G.M. Glenn, A.P. Klamczynski, W.J. Orts, L.H.C. Mattoso, United States Patent. Patent No.: US 8,641,960 B1, 2014.
[36] G.C. Dadol, A. Kilic, L.D. Tijing, K.J.A. Lim, L.K. Cabatingan, N.P.B. Tan, E. Stojanovska, Y. Polat, Solution blow spinning (SBS) and SBS-spun nanofibers: Materials, methods, and applications, Mater. Today Commun. 25 (2020), https://doi.org/10.1016/j.mtcomm.2020.101656 101656.
[37] J. Song, Z. Li, H. Wu, Blowspinning: A New Choice for Nanofibers, ACS Appl. Mater. Interfaces. 12 (2020) 33447–33464, https://doi.org/10.1021/acsami.0c05740.
[38] J.L. Daristotle, A.M. Behrens, A.D. Sandler, P. Kofinas, A Review of the Fundamental Principles and Applications of Solution Blow Spinning, ACS Appl. Mater. Interfaces. 8 (2016) 34951–34963, https://doi.org/10.1021/acsami.6b12994.
[39] F.T.G. Dias, S.P. Rempel, L.D. Agnol, O. Bianchi, The main blow spun polymer systems: processing conditions and applications, J. Polym. Res. 27 (2020) 16–18, https://doi.org/10.1007/s10965-020-02173-7.
[40] A. Barhoum, K. Pal, H. Rahier, H. Uludag, I.S. Kim, M. Bechelany, Nanofibers as new-generation materials: From spinning and nano-spinning fabrication techniques to emerging applications, Appl. Mater. Today. 17 (2019) 1–35, https://doi.org/10.1016/j.apmt.2019.06.015.
[41] J.E. Oliveira, L.H.C. Mattoso, W.J. Orts, E.S. Medeiros, Structural and morphological characterization of micro and nanofibers produced by electrospinning and solution blow spinning: A comparative study, Adv. Mater. Sci. Eng. 2013 (2013), https://doi.org/10.1155/2013/409572.
[42] A. Kasiri, J.E. Domínguez, J. González-Benito, Morphology optimization of solution blow spun polystyrene to obtain superhydrophobic materials with high ability of oil absorption, Polym. Test. 91 (2020), https://doi.org/10.1016/j.polymertesting.2020.106859.
[43] J. González-Benito, D. Torres, C. Ballesteros, V.M. Ruiz, J. Teno, PVDF based nanocomposites produced by solution blow spinning, structure and morphology induced by the presence of MWCNT and their consequences on some properties, Colloid Polym. Sci. 297 (2019) 1105–1118, https://doi.org/10.1007/s00396-019-04530-5.
[44] J.E. Domínguez, A. Kasiri, J. González-Benito, Wettability behavior of solution blow spun polysulfone by controlling morphology, J. Appl. Polym. Sci. 138 (2021), https://doi.org/10.1002/app.50200.
[45] D.D. da S. Parize, J.E. de Oliveira, T. Williams, D. Wood, R. de J. Avena-Bustillos, A.P. Klamczynski, G.M. Glenn, J.M. Marconcini, L.H.C. Mattoso, Solution blow spun nanocomposites of poly(lactic acid)/cellulose nanocrystals from Eucalyptus kraft pulp, Carbohydr. Polym. 174 (2017) 923–932. https://doi.org/10.1016/j.carbpol.2017.07.019.
[46] J. Teno, G. González-Gaitano, J. González-Benito, Poly (ethylene-co-vinyl acetate) films prepared by solution blow spinning: Surface characterization and its relation with E. coli adhesion, Polym. Test. 60 (2017) 140–148, https://doi.org/10.1016/j.polymertesting.2017.03.020.
[47] M. Iorio, J. Teno, M. Nicolás, R. García-González, V.H. Peláez, G. González-Gaitano, J. González-Benito, Conformational changes on PMMA induced by the presence of TiO2 nanoparticles and the processing by Solution Blow Spinning, Colloid Polym. Sci. 296 (2018) 461–469, https://doi.org/10.1007/s00396-018-4268-0.
[48] J. Teno, G. González-Gaitano, J. González-Benito, Nanofibrous polysulfone/TiO2 nanocomposites: Surface properties and their relation with E. coli adhesion, J. Polym. Sci. Part B Polym. Phys. 55 (2017) 1575–1584, https://doi.org/10.1002/polb.24404.
[49] J.L. Daristotle, L.W. Lau, M. Erdi, J. Hunter, A. Djoum, P. Srinivasan, X. Wu, M. Basu, O.B. Ayyub, A.D. Sandler, P. Kofinas, Sprayable and biodegradable, intrinsically adhesive wound dressing with antimicrobial properties, Bioeng. Transl. Med. 5 (2020) 1–12, https://doi.org/10.1002/btm2.10149.
[50] C. Shen, Z. Yang, J. Rao, J. Li, D. Wu, Y. He, K. Chen, Development of a thermally conductive and antimicrobial nanofibrous mat for the cold chain packaging of fruits and vegetables, Mater. Des. 221 (2022), https://doi.org/10.1016/j.matdes.2022.110931.
[51] G.C. Dadol, K.J.A. Lim, L.K. Cabatingan, N.P.B. Tan, Solution blow spinning-polyacrylonitrile-assisted cellulose acetate nanofiber membrane, Nanotechnology 31 (2020), https://doi.org/10.1088/1361-6528/ab90b4.
[52] L. Yan, X. Yang, Y. Zhang, Y. Wu, Z. Cheng, S.B. Darling, L. Shao, Porous Janus materials with unique asymmetries and functionality, Mater. Today. 51 (2021) 626–647, https://doi.org/10.1016/j.mattod.2021.07.001.

[53] Y. Ye, Y. Mao, Vapor-based synthesis and micropatterning of Janus thin films with distinct surface wettability and mechanical robustness, RSC Adv. (2017) 24569–24575, https://doi.org/10.1039/c7ra03386a.
[54] M. Wang, R. Ge, P. Zhao, G.R. Williams, D.-G. Yu, S. Annie Bligh, Exploring wettability difference-driven wetting by utilizing electrospun chimeric Janus microfiber comprising cellulose acetate and polyvinylpyrrolidone, Mater. Des. 226 (2023) 111652. https://doi.org/10.1016/j.matdes.2023.111652.
[55] Y. Shi, M. Zhou, S. Zhao, H. Li, W. Wang, J. Cheng, L. Jin, Y. Wang, Janus amphiphilic nanofiber membranes synergistically drive antibacterial and anti-inflammatory strategies for skin wound healing, Mater. Des. (2023), https://doi.org/10.1016/j.matdes.2023.111778.
[56] J.E. Domínguez, E. Olivos, C. Vázquez, J.M. Rivera, R. Hernández-Cortes, J. González-Benito, Automated low-cost device to produce sub-micrometric polymer fibers based on blow spun method, HardwareX. 10 (2021) e00218.
[57] H. Ku, C. Tu, Isobaric vapor – liquid equilibria for mixtures of acetone, ethanol, and 2,2,4-trimethylpentane at 101.3 kPa, Fluid Phase Equilib. 231 (2005) 99–108. https://doi.org/10.1016/j.fluid.2005.01.007.
[58] W.J. Moore, Physical Chemistry, Third Edit, Prentice-Hall Inc., 1962.
[59] E. Huang, A. Skoufis, T. Denning, J. Qi, R.R. Dagastine, R.F. Tabor, J.D. Berry, OpenDrop : Open-source software for pendant drop tensiometry & contact angle measurements, J. Open Source Softw. 6 (2021) 10–12. https://doi.org/10.21105/joss.02604.
[60] J.D. Berry, M.J. Neeson, R.R. Dagastine, D.Y.C. Chan, R.F. Tabor, Journal of Colloid and Interface Science Measurement of surface and interfacial tension using pendant drop tensiometry, J. Colloid Interface Sci. 454 (2015) 226–237, https://doi.org/10.1016/j.jcis.2015.05.012.
[61] D.A. Cerqueira, G.R. Filho, R.M.N. Assunção, A New Value for the Heat of Fusion of a Perfect Crystal of Cellulose Acetate, Polym. Bull. 56 (2006) 475–484, https://doi.org/10.1007/s00289-006-0511-9.
[62] K. Dimic-Misic, M.M. Kostic, O. Bratislav, M. Kuraica, A. Kramar, M. Imani, P. Gane, Iso- and Anisotropic Etching of Micro Nanofibrillated Cellulose Films by Sequential Oxygen and Nitrogen Gas Plasma Exposure for Tunable Wettability on Crystalline and Amorphous Regions, Materials 14 (2021) 3571.
[63] R.T. Paschoalin, D. Gaspar, K. Miranda, P.I.C. Claro, O.N. Oliveira, R. Martins, J.M. Marconcini, E. Fortunato, L.H.C. Mattoso, Ionic Conductive Cellulose Mats by Solution Blow Spinning as Substrate and a Dielectric Interstrate Layer for Flexible Electronics, ACS Appl. Mater. Interfaces. 13 (2021) 26237–26246, https://doi.org/10.1021/acsami.1c06274.
[64] M.H. El-Newehy, H. El-Hamshary, W.M. Salem, Solution blowing spinning technology towards green development of urea sensor nanofibers immobilized with hydrazone probe, Polymers 13 (2021) 1–14, https://doi.org/10.3390/polym13040531.
[65] C. Wang, Y. Wang, T. Hashimoto, Impact of Entanglement Density on Solution Electrospinning: A Phenomenological Model for Fiber Diameter, Macromolecules 49 (2016) 7985–7996, https://doi.org/10.1021/acs.macromol.6b00519.
[66] J. Shawe, R. Riesen, J. Widmann, M. Schubnell, UserCom 1/2000, 2000. https://www.eng.uc.edu/~beaucag/Classes/Characterization/DSCParts/Artifacts in DSC Usercom_11.pdf.
[67] J.F. Kennedy, G.O. Phillips, P.A. Williams, L. Piculell, eds., Cellucon '93 proceedings Cellulose and cellulose derivatives: Physico-chemical aspects and industrial applications, in: Woodhead Publishing Limited, 1995.
[68] P. Zugenmaier, Characteristics of cellulose acetate, Macromol. Symp. 208 (2004) 81–166, https://doi.org/10.1002/masy.200450407.
[69] K. Garg, G.L. Bowlin, Electrospinning jets and nanofibrous structures, Biomicrofluidics 5 (2011), https://doi.org/10.1063/1.3567097 013403.
[70] H. Zhao, H. Chi, Electrospun Bead-on-String Fibers: Useless or Something of Value?, in: Nov. Asp. Nanofibers, Intech, 2018: pp. 87–10, https://doi.org/10.5772/intechopen.74661.
[71] S. Huan, G. Liu, G. Han, W. Cheng, Z. Fu, Q. Wu, Q. Wang, Effect of Experimental Parameters on Morphological, Mechanical and Hydrophobic Properties of Electrospun Polystyrene Fibers, Materials (Basel). 8 (2015) 2718–2734, https://doi.org/10.3390/ma8052718.
[72] Y. Wang, C. Lai, X. Wang, Y. Liu, H. Hu, Y. Guo, K. Ma, B. Fei, J.H. Xin, Beads-on-String Structured Nanofibers for Smart and Reversible Oil/ Water Separation with Outstanding Antifouling Property, ACS Appl. Mater. Interfaces. 8 (2016) 25612–25620, https://doi.org/10.1021/acsami.6b08747.
[73] A.S. Figueiredo, A.R. Garcia, M. Minhalma, L. Ilharco, M.N. De Pinho, The ultrafiltration performance of cellulose acetate asymmetric membranes: A new perspective on the correlation with the infrared spectra, J. Membr. Sci. Res. 6 (2020) 70–80. https://doi.org/10.22079/JMSR.2019.110424.1269.
[74] M. Schwanninger, J.C. Rodrigues, H. Pereira, B. Hinterstoisser, Effects of short-time vibratory ball milling on the shape of FT-IR spectra of wood and cellulose, Vib. Spectrosc. 36 (2004) 23–40, https://doi.org/10.1016/j.vibspec.2004.02.003.
[75] H. Zhou, Z. Guo, Superwetting Janus membranes: Focusing on unidirectional transport behaviors and multiple applications, J. Mater. Chem. A. 7 (2019) 12921–12950, https://doi.org/10.1039/c9ta02682g.
[76] L.A. Goetz, N. Naseri, S.S. Nair, Z. Karim, A.P. Mathew, All cellulose electrospun water purification membranes nanotextured using cellulose nanocrystals, Cellul. 25 (2018) 3011–3023, https://doi.org/10.1007/s10570-018-1751-1.
[77] A. Barazesh, M. Navidbakhsh, A. Abouei Mehrizi, M. Koosha, S. Razavi Bazaz, T. Li, Simultaneous Modeling of Young's Modulus, Yield Stress, and Rupture Strain of Gelatin/Cellulose Acetate Microfibrous/Nanofibrous Scaffolds Using RSM, Front. Bioeng. Biotechnol. 9 (2021) 1–16, https://doi.org/10.3389/fbioe.2021.718718.